Engineering Structures 245 (2021) 112971

Contents lists available at ScienceDirect

Engineering Structures

journal homepage: www.elsevier.com/locate/engstruct

Developing data-driven surrogate models for holistic performance-based assessment of mid-rise RC frame buildings at early design

Mohsen Zaker Esteghamati *, Madeleine M. Flint

Department of Civil and Environmental Engineering, Virginia Polytechnic and State University, Blacksburg, VA, United States

ARTICLE INFO

Keyword:
Surrogate modelling
Early design
Variance-based sensitivity
Interpretable Machine learning
Performance-based Engineering

ABSTRACT

This paper presents a framework to develop generalizable surrogate models to predict seismic vulnerability and environmental impacts of a class of buildings at a particular location. To this end, surrogate models are trained on a performance inventory, here simulation-based seismic and environmental assessments of 720 mid-rise concrete office buildings of variable topology in Charleston, South Carolina. Five surrogate models of multiple regression, random forest, extreme gradient boosting, support vector machine and k-nearest neighbors were trained in a machine-learning pipeline including hyperparameter tuning and cross-validation. Variance-based sensitivity and accumulated local effect analysis were performed on the most accurate model to identify the most influential parameters and interpret the trained surrogate model. Support vector machines achieved the highest accuracy for total annual loss with an average 10-fold adjusted R^2 of 0.96, whereas simpler linear regression was adequate to estimate the initial and seismic-induced embodied carbon emission. Floor area, building height, lateral-resisting frame weight, and average beam section sizes were found to be the most influential features. As these features may be approximated by an experienced structural engineer the results indicate that, with suitable performance inventories available, it should be possible to employ surrogate models in early design to narrow the initial design space to highly resilient and sustainable configurations.

1. Introduction

Improving resiliency requires new design and assessment methods that can link buildings' physical characteristics, such as material and topology, to their performance under natural hazards and long-term post-event behavior. Performance-based engineering (PBE) [1–3] provides a rigorous probabilistic approach to characterize hazards, measure their impact on building response, and relates the resultant response (such as deformation demands) decision variables. Fully-probabilistic PBE has been introduced to assess the impacts of different hazards such as earthquake [2,4], fire [5–7], post-earthquake fire [8,9], tsunami [10], wind [11] and hurricane [12] on the built environment. Among these frameworks, performance-based earthquake engineering (PBEE) has been more frequently used to evaluate the vulnerability of critical infrastructures such as nuclear power plants[13], bridges [14,15], and transportation networks [16]. Nevertheless, PBEE is still not a common design tool for mid-rise commercial buildings due to the computational burden and required expertise for hazard and structural modeling. PBEE application at earlier stages of design (e.g. schematic design) poses an even greater challenge.

Early design defines a design problem, identifies its parameters, and explores their interaction, and perhaps, is the key stage to shape the building's resiliency [17], since the designer has the freedom and flexibility to consider a broad array of topologies, subsystems, and materials. The ability to link those conceptual alternatives to their long-term consequences in terms of societal goals such as resiliency and sustainability would represent a significant advancement beyond traditional heuristics [18]. On the other hand, the implementation of performance-based approaches exacerbates in early design due to its dynamic and fast-paced nature, lack of design details, and imprecise exposure and operation data [19–21]. An early design framework was recently proposed that uses simplified hand calculations to relate geometry and material to seismic performance objectives [22]. The proposed framework was later extended to account for collapse risk [23], and supplemented with a closed-form relationship to derive structural response subjected to earthquake hazard [24]. This framework suggests that certain aspects of seismic performance (e.g., yield displacement) are only related to geometry, emphasizing a relationship between topology

* Corresponding author.
E-mail addresses: mohsenzaker@vt.edu (M. Zaker Esteghamati), mflint@vt.edu (M.M. Flint).

https://doi.org/10.1016/j.engstruct.2021.112971
Received 7 April 2021; Received in revised form 18 July 2021; Accepted 7 August 2021
Available online 12 August 2021

and hazard performance.

Surrogate modeling constructs a mathematical model to characterize the response of nonlinear complex systems and can substitute computationally expensive simulations, such as ones required by PBE, with low-cost input–output mapping. Data-driven surrogate modeling offers a fresh perspective to address the diversity of the early design space, the large uncertainties involved in the performance estimation, and the computational burden of performance-based design. With increased high-performing computational capacities, numerical simulations can be performed to obtain performance for a limited set of design space points. Aggregation and synthesis with existing assessments [25] and the knowledge base for similar design problems can provide adequate data to form a performance inventory. By using this performance inventory to train a (or multiple) surrogate model(s) it is possible to rapidly estimate performance over the complete design space. Deploying this approach in early design, however, requires that sufficiently accurate predictions be obtained from input parameters known or feasibly estimated during this stage.

This study presents a framework to develop data-driven surrogate models to facilitate a holistic performance-based early design (PBED), here derived for mid-rise concrete commercial buildings. The underlying notion of this framework lies in compiling a performance inventory for a class of buildings to facilitate the learning process of generalizable surrogate models. The trained surrogate models are then used to relate crude topological and design parameters to performance endpoints, such as seismic economic loss and carbon emission. The application of surrogate modeling in this study differs from prior work in three aspects. First, rather than implementing surrogate models to characterize a single building design for optimization, the intended goal is to derive generalizable surrogate models for a class of buildings. Second, using crude features (such as ones related to general topology) increases surrogate models' suitability for early design. Third, translating design decision consequences in terms of performance endpoints (as opposed to midpoint indicators such as structural responses) enhances communication and risk-informed decision-making in an architecture-engineering-construction (AEC) team comprising individuals from diverse backgrounds. After reviewing literature on application of surrogate modeling in PBE, this paper develops a seismic and environmental performance inventory, describes the proposed machine-learning pipeline, and compares results and sensitivity and interpretation of the best surrogate models.

2. Literature review

The literature on surrogate modeling application in PBE encompasses a broad spectrum of modeling approaches ranging from mechanistic (sometimes referred to as physics-based) to data-driven methods. Mechanistic-based approaches use classical mechanics and structural dynamics theory and are more frequently used in practice due to their intuitiveness and presumed generalizability [26,27]. In contrast, despite data-driven surrogate modeling's wide implementation in optimization and uncertainty quantification of complex dynamic systems [28–31], its application in PBE assessment of built environment is limited [32–34]. Table 1 provides several recent studies exploring data-driven surrogate modeling in PBE applications. The application of data-driven surrogate modeling in seismic performance estimation has a relatively longer history than other hazards, as a method to estimate seismic demand models for the full spectrum of the site's hazard. These surrogate models aimed to predict engineering demand parameters (EDPs) for a set of structural properties (e.g. damping, stiffness) and ground motion intensity measures (IMs). In this context, the linear regression that relates structure's deformation to ground motion's spectral value, is a data-driven surrogate model as it *predicts* structure's response at points where simulation hasn't been performed [35]. However, the term *data-driven surrogate modeling* is mostly used to refer to cases where multiple predictors (or features) are related to a single or multiple response(s).

Adopting the more common definition, the application of data-driven surrogate models initiated in seismic assessment of highway bridges. Seo and Linzell used the response surface method to construct fragility curves for curved steel bridges based on eleven parameters covering bridge geometry and material properties [36]. Manghathlu et al. used the artificial neural network (ANN) to derive multidimensional seismic fragility of box-girder bridges with single- and two-column bents [37]. Several studies used surrogate models to assess bridge performance under other hazards than earthquakes. Ataei and Padgett applied support vector machine (SVM), random forest (RF) and logistic regression to estimate deck unseating failure of coastal bridged under hurricane loads, and concluded while three methods have reasonable accuracy, RF provided the least misclassification [38].

Despite data-driven surrogate modeling prevalence in bridge seismic assessment, limited studies employed them for buildings performance. Zou et al. used kriging to relate structural properties of wood wall building and ground motion shaking to median drift values and collapse probability [47]. Hwang et al. developed surrogate models to predict drift demand of 4- and 8-story RC buildings considering uncertainties in modeling parameters and concluded that boosting algorithms outperform others [48]. Mitropoulou and Papadrakakis used ANN to estimate structural demand using incremental dynamic analysis for two 5- and 8-story 3D RC buildings [49]. Gidaris et al. used kriging to estimate a 4-story RC building with fluid dampers under a stochastic ground motion model and derived its drift hazard curves [50]. Möller et al employed three surrogate models of the polynomial response surface, local interpolation, and ANN to predict the structural response (e.g. drift) and damage indices of a 5-story RC frame subjected to earthquake loads. They concluded that ANN outperforms other methods, while all three can have reasonable accuracy [51]. Gentile and Galasso applied Gaussian process regression (GPR) to derive seismic fragility for school building portfolio based on nonlinear static analysis and concluded that GPR shows high prediction power [52].

Recently, several studies extended data-driven surrogate modeling

Table 1
Recent literature on data-driven surrogate modeling for PBE applications.

Study	Year	Structure	Hazard	Response	Surrogate Model [a]
Zhong et al. [39]	2020	Cable-stayed bridge	Earthquake	Pylon, Curvature ductility, bearing deformation, cable axial force,	GPR
Bernier & Padgett [40]	2019	Storage tanks	Surge, Wave, wind	Failure probability (buckling, dislocation)	Logistic regression
Le & Caracoglia [41]	2020	Monopole	Tornado	Probability of failure	ANN
Javidan et al. [42]	2018	3-story steel frame	Vehicle collision	Beams rotational demands	ANN
Fang et al. [43]	2020	Cable-stayed bridge	Wind, wave	Root mean square values of lateral displacement	SVR, BPN, GPR
Micheli et al [44]	2020	A 39-story steel building	Wind	Peak drift and acceleration	Kriging, adaptive wavelet network
Li & Caracoglia [45]	2019	Wind turbine blades	Wind	Flutter analysis responses	Stochastic collocation
Wilkie & Galasso[46]	2021	Offshore wind turbine	Wind	Load-induced fatigue	GPR

[a] **GPR**: Gaussian Process regression, **ANN**: Artificial neural network, **SVR**: support vector machine.

for wind hazard. Micheli et al. implemented surrogate modeling for the performance-based design of a wind-excited tall building. Instead of a single high-dimensional model, they used multiple kriging-based surrogate models, each representing the dynamic response of a single floor of the 40-story building [53]. In a different study, Micheli et al. compared kriging and adaptive wavelet network surrogate models to estimate acceleration responses of a 39-story wind-excited tall building with friction devices, and concluded that both models yield similar accuracy [44].

The reviewed literatures suggests that the application of data-driven surrogate modeling to risk-based assessments of buildings is still at early stages, as the previous studies mainly focused on feasibility of predicting structural responses of a test-bed building (or multiple buildings) using high-resolution input parameters. To apply data-driven surrogate models at early design, additional studies are needed to determine whether these models can identify optimal designs with reasonable accuracy using limited data, and be generalized to a class of buildings with varying topology and dynamic characteristics.

3. Performance inventory development

This section describes the procedure used to develop a multi-dimensional performance inventory for mid-rise concrete frame office buildings. As shown in Fig. 1, the first step in performance inventory development is sampling from the design parameters space, generating admissible designs to populate the inventory, and constructing numerical models to estimate performance through relevant analysis procedures.

3.1. Early design parameters sampling

To illustrate the proposed framework, early design of planar

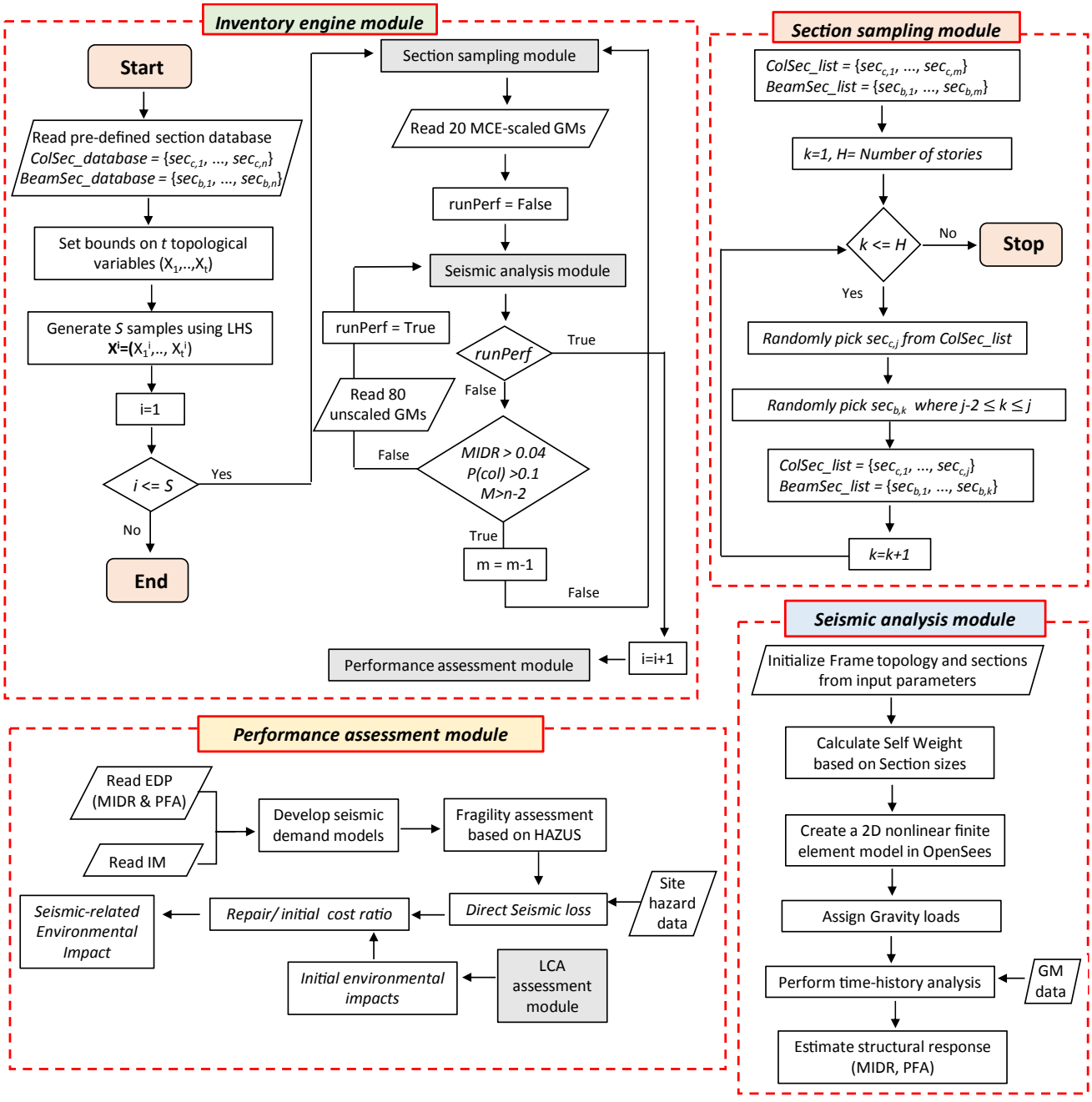

Fig. 1. Flowchart of the inventory development.

symmetric concrete frame buildings was studied. Concrete moment-resisting frames (MRFs) are prevalent in earthquake-resistant design due to significant ductility and providing more flexibility for architectural design [54]. To create a generalizable performance space, the archetype building concept is adopted [55,56], where the material properties and some topological features (e.g. overall rectangular plan, no horizontal or vertical irregularity) are kept similar to represent a class of buildings.

The archetype concrete frame office shown in Fig. 2 can be described through four topological parameters: number of bays in the x-direction, number of bays in the y-direction, bay length, and number of floors. A Latin Hypercube Sampling scheme was employed for the four mentioned parameters, where the parameters are assumed to be independent. Following guidelines and MRF design practice [54], bay length was considered to be from 21*ft* to 30 *ft* with 3 *ft* intervals. Story number ranges from 3 to 6 stories, where the first story's and other stories height are 14 *ft* and 12 *ft*, respectively. The number of bays in each direction varies between 2 and 6. All the buildings are assumed to be located in Charleston, South Carolina, USA (32.7221, −79.9341). The buildings are exposed to high seismic hazard with an $S_{DS} = 0.75\ g$ (i.e., design spectral response acceleration at short periods) and site class B/C boundary (associated with rock/dense soil) [57]. Only the perimeter frames resist lateral loads, whereas the interiors frames support gravity loads. It should be noted that while the simple geometric representation of this class of buildings removes nuances of a more realistic design project from the proposed framework, nevertheless, the demonstrated procedure is readily extendable to other classes of buildings, design problem or hazards.

3.2. Seismic design and modeling

Fig. 1 shows the pseudo-directional algorithm used to automate populating design space. Each topological sampling point from Latin Hypercube Sampling is paired with twelve different design alternatives in terms of different combinations of beams' and columns' sections. The design variations are an outcome of the "*section sampling*" module which applies MRF design principles to a predefined list of code-conforming concrete beam and column sections that are checked based on longitudinal and transverse reinforcement sizing and spacing requirements [58].

In the first iteration, the section sampling module chooses a column section from the column list for the first floor, and subsequently picks a smaller or equal beam section for the beams of the same floor. The predefined section lists are compiled so that for any beam and column sections of the same dimensions, the beam section has relatively smaller reinforcement ratio. The combination of these rules ensures that at each frame connection the selected beams are weaker than the column, implicitly considering the strong-column weak-beam requirement. Next, the selected sections are removed from the list, and the algorithm picks a smaller column section for the upper floors, and subsequently continues on the inner loop to pick beam sections as was previously discussed. The second rule ensures that stronger sections are assigned to lower floors that are expected to sustain a larger lateral load. The completed section list is paired with topological parameters and passed as input to a "*seismic analysis*" module.

The seismic analysis module first constructs a nonlinear finite element model of the frame as shown in Fig. 2.b. Since the strength and stiffness degradation of frame members' degradation is a key factor to determine moment frames' global performance, a concentrated plasticity model is implemented in OpenSees [59], where beams and columns are represented with elastic members with two nonlinear plastic hinges at both ends. The monotonic backbone curve of nonlinear hinges is defined using three pairs of strength-deformation values based on regression equations by Haselton et al. [60]. In addition, cycle deterioration of strength and stiffness is included. Both components' geometric nonlinearities and P-Δ effects are included in analytical models. P-Δ is accounted by a fictitious leaning column [61] that is connected to the main frame by truss elements, where the column is adjusted to have small stiffness to remove leaning column lateral stiffness.

The seismic analysis module then applies 20 site-specific ground motions that are scaled to the maximum considered earthquake (MCE) level. These GMs are a subset of a larger synthetic GM suite of 80 records. To obtain this GM suite, a geologically-realistic probabilistic seismic hazard analysis of Charleston was used as the input for a stochastic GM simulation. Hazard scenarios in terms of magnitude and distance were derived using an inverse transform sampling from the hazard deaggregation at each level, such that the number of pairs in each bin was proportional to that bin's contribution to the hazard [62]. Subsequently, for each magnitude-distance pair and associated hazard level, a synthetic GM record is generated.

Structural response in terms of maximum inter-story drift is recorded and if (*i*) all floors do not exceed a drift value of 4% [63], and (*ii*) a maximum number of 2 collapses occur (10% collapse probability under MCE), the design is deemed acceptable and a second set of analysis with the whole 80 unscaled GMs is performed to obtain structure's drift and acceleration responses for loss assessment. Otherwise, the algorithm removes the smallest beam and column sections from the pre-defined list and returns to the section sampling module to pick a new design using the adjusted list. For each topological parameter, the algorithm generates 12 design variations, resulting in a total design space of 720 frames (60 topology parameters × 12 design). It should be emphasized that the objective of the section sampling algorithm is to account for the

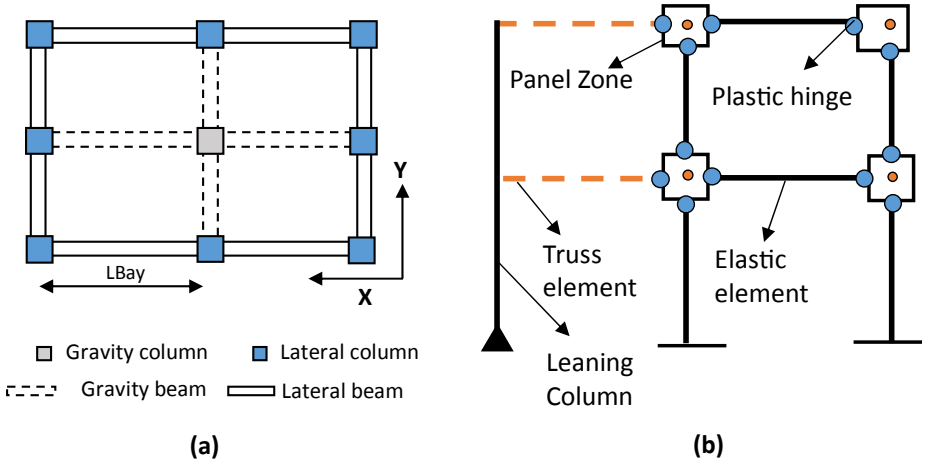

Fig. 2. (a) Plan layout (b) nonlinear model configuration.

variability of seismic design rather than an automated careful seismic design, which is beyond the scope of this paper and can be found elsewhere [55]. Additionally, the algorithm ensures that, compared to a random section selection, relatively more admissible design samples are generated, hence reducing runtime to develop a performance inventory.

3.3. Seismic loss evaluation

Seismic loss was derived following an assembly-based approach where structural peak drift and acceleration responses are mapped to structural, drift-sensitive nonstructural, and acceleration-sensitive nonstructural global damage based on the Hazus-MH guidelines [64]. This approach simplifies loss calculation as it lumps all building components into assembly categories [65], reducing the required information that is needed in a rigorous component-based approach. Following Ramirez et al. [66], the expected total seismic loss (L_T) is decomposed to collapse-related (L_C) and non-collapse (L_{NC}) losses as follows:

$$E(L_T|IM) = E(L_{NC}|IM)(1 - P(C|IM)) + E(L_C|IM)P(C|IM) \quad (1)$$

where E($X|Y$) is the expected value of random variable X conditioned on Y, and P(X) shows the probability of random variable X. The non-collapse loss is then disaggregated to structural (L_S), drift-sensitive nonstructural ($L_{NS,DS}$), and acceleration-sensitive nonstructural assemblies ($L_{NS,AS}$).

Seismic fragilities are defined as the conditional probability of EDP exceeding the HAZUS's global damage states in terms of EDP thresholds. Following [67], linear and logistic regression methods were used to estimate the fragilities for non-collapse and collapse cases, respectively. The critical EDP value corresponding to collapse was taken as a drift value of 10% based on suggested values for moment frames [68].

To consider all possible site hazard level's impact, the expected loss is integrated over the site's hazard in term of hazard intensity measure (IM) to derive expected annual loss (EAL) as follows:

$$\lambda(L_T) = \int_{IM}^{0} E(L_T|IM).\left|\frac{d\lambda(IM)}{dIM}\right| dIM \quad (2)$$

Hazus-MH describes loss values as a ratio of building replacement cost. To convert these percentages to monetary loss values, a replacement cost of 185 USD/ft^2 was adopted for concrete frames in Charleston [69]. Section 6 provides additional discussion on the sensitivity of results to building cost values and assumptions.

3.4. Environmental impact modeling

A holistic early design must evaluate different alternatives across multiple performance domains of economic, natural hazards, and environmental [70,71]. As an illustration, the initial environmental impact of the developed office inventory was assessed using a process-based whole building life cycle assessment (LCA) based on ISO14400 in Athena Impact Estimator [72]. As shown in Fig. 3, the LCA boundary included the main structural frame, floors, interior partitions and exterior envelope. The amount of concrete material in the structural elements was calculated based on the section sampling module of the performance inventory described in Section 3.2. The interior partition walls quantity is calculated using the FEMA P-58 normative quantity estimation tool based on building floor area and occupancy [73]. Following Charleston Board of Architectural Review regulations, the exterior envelope consists of concrete masonry blocks with brick veneer with a window to wall ratio of 0.31. LCA was carried out for a service life of 50 years for the functional unit of the whole building. In a process-based LCA, different building life cycle stages are disintegrated into processes that map input material and energy to the emission and waste. Here, production, construction, and end-of-life stages were included in analysis, whereas the use phase was limited to maintenance. Although the operational energy use dominates life cycle impacts [74,75], it is excluded from the LCA, as related factors, such as shading, utilities schedule, and mechanical equipment, are assumed to be consistent

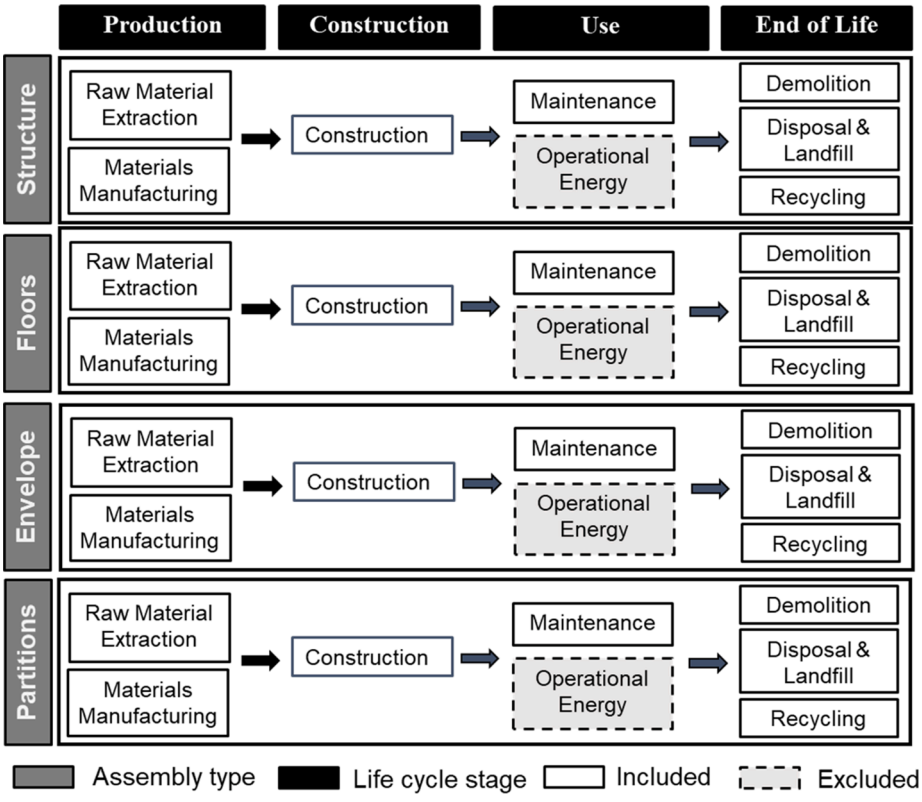

Fig. 3. LCA analysis boundary to derive initial environmental impacts.

between different designs. In addition, any process not directly related to frame construction was excluded such as temporary nonstructural elements and manufacturing goods needed for construction products.

After an earthquake, buildings are assumed to be rehabilitated, which impacts the environment due to materials consumption and energy use. Earthquake-induced environmental impacts were calculated by applying the cost ratio (i.e. seismic-related repair costs to the total building cost) to the initial impacts, based on [76]. This approach assumes that the same labor and material cost is used for both repair and production, which is not often the case, particularly for partial repairs. Therefore, for low seismic damage levels, it will lead to a near perfect correlation to initial material cost. This issue will be further discussed in Section 5. Among different environmental impact measures, global warming potential (GWP) in terms of equivalent carbon emission is considered.

4. Surrogate modeling workflow

This section describes the procedure to develop a suite of surrogate models to predict performance end-points in terms of expected seismic loss and environmental perfor mance. A schematic overview of surrogate modeling development is shown in Fig. 4.

4.1. Feature selection

A set of 17 candidate early design parameters were selected to represent building topology and design. It was decided to (i) only include parameters that the designer can assume without additional effort at this stage, and (ii) avoid categorical variables that reduce the efficiency of ML algorithms. The topological parameters include building height (Height), building dimension in X (Xdim) and Y (Ydim) dimension, bay length (LBay), floor area (FlrArea), aspect ratio (AspectRat), number of columns (ColNum) and beams (BeamNum). The parameters associated with the design cover lateral-resisting frame (LatWeight) and total building weight (TotalWeight), average column (ColAvg) and beam areas (BeamAvg), first story column (ColSec1) and beam (BeamSec1) area, average column (rhoColAvg) and beams (rhoBeamAvg) reinforcement ratio, and first story column (rhoCol1) and beam reinforcement (rhoBeam1) ratios. It should be noted that while more precise parameters (such as structural period) could strongly improve model accuracy, they are usually not available at preliminary stages without performing additional analysis.

Fig. 5 shows the correlation values between all candidate features. Intuitively, variables describing beam and column section sizes are highly correlated to each other, while being moderately correlated to building footprint variables. In addition, they have a small negative correlation to reinforcement variables. Except for height and bay's length, topological parameters are highly correlated, whereas they are not correlated to reinforcement variables.

A comprehensive feature selection approach would build models with all different combinations of features, however, such a brute force approach is not feasible for a large number of parameters. As shown in Fig. 4, instead, statistical methods (F-values and mutual information gain) were used to determine the features that are highly related to a given response. Additionally, an iterative tree-based feature selection method was also employed to determine the minimum number of features yielding the highest accuracy. Based on the insights provided by these methods, a variety of subsets are generated and examined as part of the model selection procedure.

4.2. Model selection & validation

A wide array of surrogate algorithms exists to map the input domain to an output real number. Each algorithm is characterized by its hyperparameters, which describe how the algorithm will learn from the dataset. Previous studies emphasized that hyperparameter calibration is essential to achieve accurate surrogate models [77]. As shown in Fig. 4, first the inventory was partitioned into 70% training and 30% testing data groups. Then, for each surrogate modeling algorithm and feature subset, a randomized search algorithm was applied to find the bounds on best-performing hyperparameters based on the training dataset, followed by a grid search algorithm to further tune hyperparameters. 3-fold cross-validation (CV) was used to avoid overfitting at each hypertuning method. A k-fold CV splits a set to k subset with equal size, trains on k-1 subset and validates on the kth set and repeats this process for k times, representing the average results.

The tuned surrogate models for each feature subset were then used to predict the testing dataset, and compared based on accuracy measures described in Section 5. Lastly, a sensitivity assessment was performed on the best tuned model for each surrogate algorithm, and a new feature subset including only the most influential features is obtained. This feature subset was then used to train a final surrogate model and compared to the best performing model to determine whether a simpler (i.e. fewer features) model with the same accuracy could be obtained.

4.3. Surrogate modeling algorithms

4.3.1. Multiple linear regression (MLR)

Multiple linear regression (MLR) is perhaps the most straightforward surrogate modeling technique, where a single response is assumed to be linearly related to multiple features as follows:

$$y = \beta_0 + \beta_1 x_1 + \cdots + \beta_n x_n + \epsilon \tag{3}$$

where ε is model error and β_0 ,…, β_m are m model parameters obtained

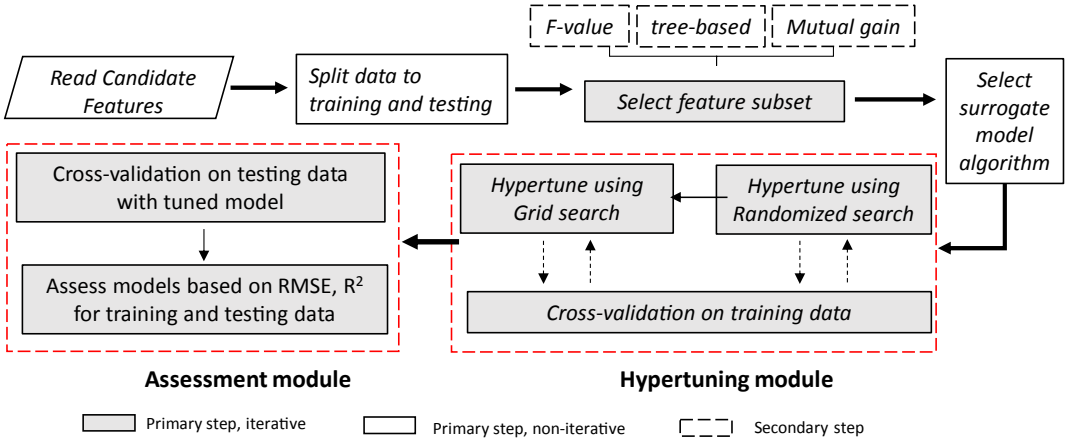

Fig. 4. Surrogate modeling pipeline.

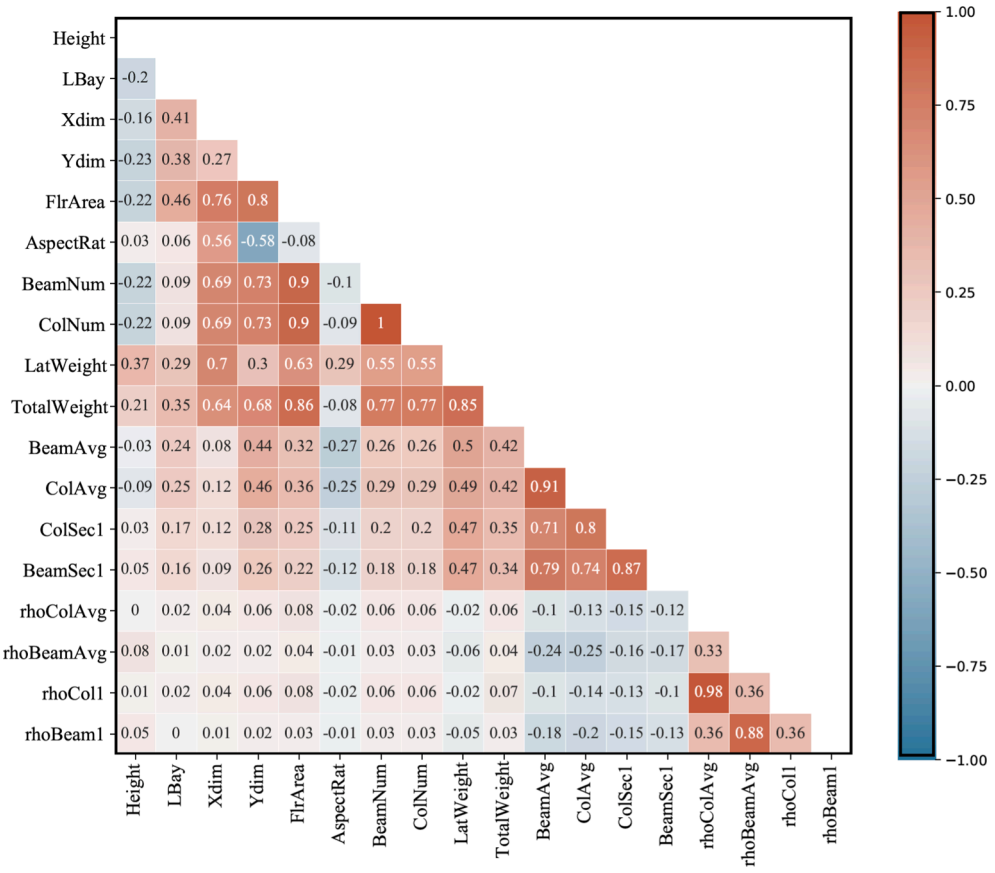

Fig. 5. Correlation map of independent features.

through minimizing the sum of squared residuals as follows [78]:

$$min \sum_{i=1}^{m} \left(y_i - \beta_0 - \beta_1 x_{1,i} - \cdots - \beta_n x_{n,i}\right)^2 \tag{4}$$

Although MLR does not need hypertuning (fast training) and is easy to implement, it shows bias if the response relationship to input is inherently nonlinear.

4.3.2. Random forest (RF)

Random forests grew on the idea of *bagging*, where the average of numerous parallel weak (i.e. noisy) models results in an unbiased model. An RF with N trees can be represented as follows [78]:

$$y(x) = \frac{1}{n} \sum_{n=1}^{N} \sum_{j=1}^{J} \gamma_j I\left(x \in R_j\right) \tag{5}$$

where the R and γ model parameters are estimated by minimizing the empirical risk as follows:

$$min \sum_{j=1}^{J} \sum_{x_i \in R_j}^{J} L\left(y_i, \gamma_j\right) \tag{6}$$

RF efficiently handles nonlinearity of response and collinearity of features, but is very sensitive to variations in training datasets, and prone to overfitting unless pruning is enforced.

4.3.3. Extreme gradient boosting (XGB)

Gradient boosting methods relies on the boosting approach, at which weak models with low bias and high variance are used in a sequence to retrain the previously trained model at each stage. XGB uses a more regularized loss function than other implementations of the gradient boosting method to limit overfitting. The objective function at iteration m is as follows [79]:

$$\min \sum_{j=1}^{n} l\left(y_i, \hat{y}_i^{(m-1)} + f_t(x_i)\right) + \Omega(f_t) \tag{7}$$

where l is the loss function measuring the difference of predicted (y_i) and observed response ($\hat{y}_i$), and Ω is the penalty term for model complexity.

Compared to RF, XGB better penalizes redundant features to avoid bias. However, XGB is also prone to overfitting and has longer training time due to the larger number of hyperparameters.

4.3.4. Support vector regression (SVR)

Support vector regression (SVR) aims to find the optimal hyperplane in the input domain that deviates at a maximum amount of ε from decision boundary lines. This can be translated to additional flexibility to assume an error margin (i.e. ε) suitable for the model, instead of minimizing the squared error in the ordinary least square method linear regression as follows [78]:

$$\begin{aligned} min\ & \frac{1}{2}\|w\|^2 + C\sum_{i=1}^{n} |\xi_i| \\ & + |\xi_i| \\ s.t. & |y_i - w_i x_i| \le \epsilon \end{aligned} \tag{8}$$

where ξ_i is the deviation from ε, C is the penalty term for points outside of the decision boundary and w is the coefficient vector.

SVR is robust against overfitting and gives flexibility through kernel selection, however it does not always scale well to large datasets. Interpreting its hyperparameters is difficult.

4.3.5. k-Nearest Neighbor (kNN)

KNN algorithms predict response for X_i (i.e. y_i) by locating the N

nearest points in input space to X_i and averaging all corresponding responses. Assuming k neighborhoods are defined, y_i is obtained as follows [80]:

$$y_i = \frac{1}{k}\sum_{X\epsilon N} y(X) \tag{9}$$

KNN has few hyperparameters to tune but is non-parametric and can result in overfitting with small training and large feature sets.

5. Comparison of developed models

Two measures of adjusted R^2 (i.e. coefficient of determination) and root mean square error (RMSE) were adopted to assess model accuracy as follows:

$$R^2_{adj} = 1 - \frac{\left(1 - \left(1 - \frac{\sum\left(y_i - \hat{y}_i\right)^2}{\sum\left(y_i - \bar{y}\right)^2}\right)\right)(n-1)}{n-k-1}$$
$$RMSE = \sqrt{\frac{1}{n}\sum\left(y_i - \hat{y}_i\right)^2} \tag{10}$$

where y_i and $\hat{y}_i$ are ith response value and its estimation using the surrogate model, $\bar{y}$ is the average response for the whole considered set, n is the number of observations and k is the number of features used in the surrogate model.

RMSE measures the standard deviation of residuals, or how on average the predicted response deviates from the predicted value, whereas, adjusted R^2 represents the amount of response variance explained by the model, and is adjusted to penalize models that introduce redundant features with an insignificant contribution. It should be noted that while accuracy measures for both training and test sets are provided, model selections are based on test set results, and training set results are used to diagnose whether overfitting or underfitting has occurred.

5.1. Seismic loss comparison

Fig. 6 shows the predicted versus observed total seismic loss value for train and test sets, and Table 2 provides the accuracy measure results. In addition to adjusted R^2 and RMSE, 10-fold R^2 are provided in Table 2 since this measure can better describe algorithm performance for future datasets. Overall, the results demonstrate that the proposed framework generated surrogate models that are able to predict the total loss for the studied class of building with reasonable accuracy. In addition, while different surrogate algorithms selected a different set of features, four features of building height, floor area, weight (total, lateral, or both) and average beam section size were selected by all models to predict total seismic loss.

Among different surrogate models, SVR and XGB outperform other models, where SVR has the highest 10-fold adjusted R^2 on the testing set and XGB has the lowest RMSE, although not substantially lower than SVR. In contrast, KNN and RF performed poorly. The notable difference between KNN RMSE on train and test sets indicates overfitting. Additional training on KNN showed that in most cases and even with minimum number of neighbors, it overfits data. On the other hand, RF has the highest standard deviation of 10-fold adjusted R^2 on test set, indicating that consistent prediction might not be achieved for different test sets. Lastly, while MLR shows high adjusted R^2 on test set, it has the highest test RMSE, which is due to MLR's poorer prediction power for small and high losses.

To investigate the source of algorithms' differing performance, Fig. 7 compares surrogate models across the constituent losses. All models have a notably lower prediction capability for collapse losses. While KNN has poor performance (low median adjusted R^2 and high interquartile range) across *all* losses, other algorithms have varying performance over loss types. The best surrogate model, SVR, has the highest performance for nonstructural and collapse losses (i.e. highest median adjusted R^2 and lowest dispersion for the nonstructural losses), whereas a relatively poor performance for structural losses. MLR can predict structural loss with reasonable accuracy, but its adjusted R^2 shows a wide range for collapse and nonstructural losses, indicating possible bias in the model. XGB performs well for structural and collapse losses but underperforms for nonstructural losses. Lastly, although RF shows relatively adequate performance for structural losses and nonstructural acceleration-sensitive losses, it has the lowest median adjusted R^2 for collapse losses, lowering its overall performance. At collapse, the structural response demonstrates significant nonlinearity and hence, the superior performance of XGB, SVR for collapse losses are not surprising as these algorithms handle nonlinearity well, whereas MLR assumption of linearity does not hold.

5.2. Environmental performance comparison

The surrogate modeling workflow (described in Section 4) was used

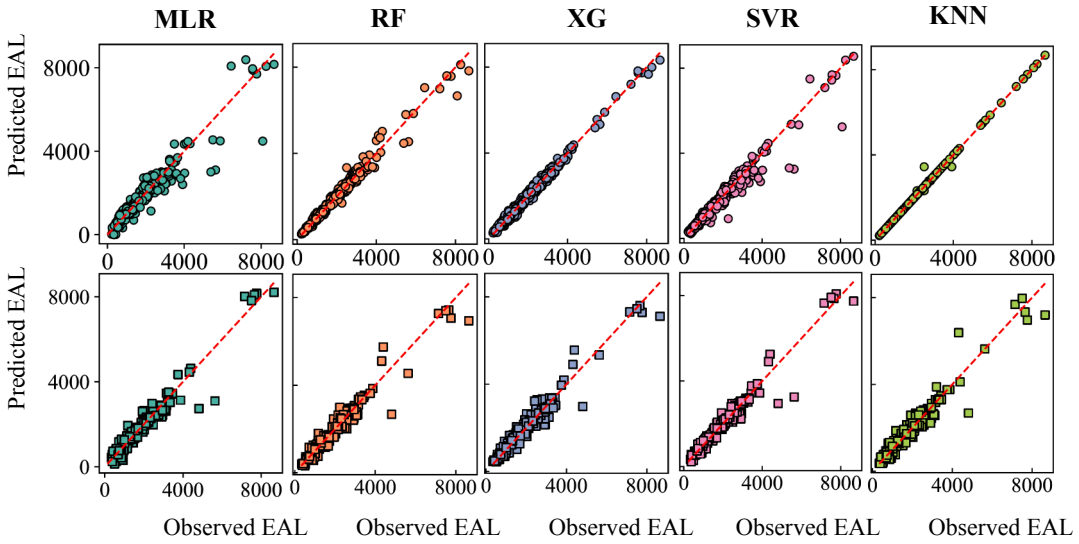

Fig. 6. Comparison of different surrogate models on training (top) and testing (bottom) sets.

Table 2
Comparison of different surrogate models to predict total loss.

Model	Features	Adjusted R^2		Adjusted R^2 (10-fold CV)				RMSE	
		Train	Test	Train		Test		Train	Test
				Mean	Std	Mean	Std		
MLR	Height, FlrArea, AspectRat, ColNum, TotalWeight, BeamAvg, BeamSec1	0.90	0.93	0.89	0.06	0.92	0.06	364	325
RF	Height, FlrArea, AspectRat, ColNum, TotalWeight, BeamAvg, BeamSec1	0.98	0.94	0.87	0.06	0.87	0.14	164	308
XGB	Height, Ydim, FlrArea, TotalWeight, ColAvg, BeamAvg, rhoCol1	0.99	0.95	0.92	0.05	0.89	0.1	115	283
SVR	Height, Ydim, FlrArea, LatWeight, BeamAvg, BeamSec1, rhoBeamAvg	0.95	0.95	0.92	0.05	0.96	0.05	272	285
KNN	Height, Xdim, Ydim, LatWeight, TotalWeight, ColAvg, BeamAvg	1.00	0.94	0.88	0.05	0.87	0.07	53	319

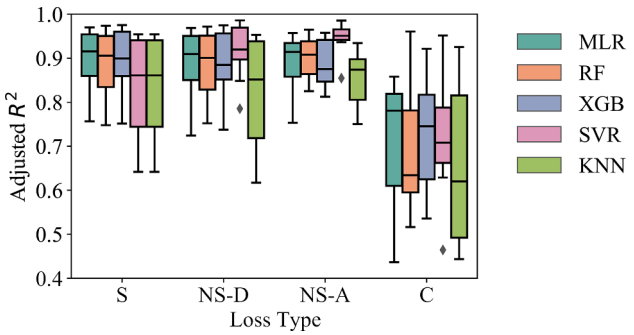

Fig. 7. Decomposing surrogate models performance for total loss to the constituent losses.

to construct data-driven models for environmental performance. As shown in Fig. 8.c, irrespective of the selected surrogate model algorithm, model development for environmental performance suggests that using only one feature (i.e., total building weight) is sufficient to represent global warming potential. This is mainly because the cost ratio method is employed (i.e., assuming a linear relationship between repair cost and environmental impacts), and the repair cost is relatively low for this site. Hence, seismic-related embodied environmental impacts are substantially smaller than initial embodied impacts. As shown in Fig. 8.a, the average seismic-induced GWP for the whole inventory is 1.1% of the initial GWP with a standard deviation of 0.19 %. Therefore, embodied GWP is dominated by the initial emissions, governed by the amount of used material (here, primarily concrete). As a result, any feature that can capture material quantity can adequately characterize embodied GWP, i.e. total building weight. Comparing between different models, while using more flexible algorithms yield smaller RMSE, the advantage of using an interpretable surrogate model outweigh smaller improvements on prediction accuracy, hence a linear regression model (Fig. 8.b) is fitted to the LCA data. The results show that each ton increase in total building weight results in 0.3 ton additional embodied CO_2 emission. It should be noted that the developed model might not hold for sites with higher seismicity or if a different method (e.g., detailed LCA modeling of each needed repair activity) is used to calculate seismic-induced impacts.

6. Sensitivity assessment

This section studies the SVR model's sensitivity to input features and subsequently attempts to interpret the relationship between total loss and selected early design parameters. Next, the sensitivity of surrogate modeling to different use scenarios is studied to determine the influence of assumptions made in this study on the surrogate model prediction.

6.1. Variance-based sensitivity assessment

In this method, the response variance, V(y) is decomposed into partial variances as follows [81]:

$$\mathrm{V(y)} = \sum_{i}^{n} \mathrm{V_i} + \sum_{i}^{n} \sum_{j>i}^{n} V_{ij} + \cdots + V_{1\cdots n} \tag{11}$$

where V_i denotes the expected reduction in the variance of the response given feature i, and V_{ij} is the expected reduction in response variance due to both features i and j, and so on. Using Sobol formula, the first-order effect (S_i) and total effect (S_T) indices are defined as follows:

$$S_i = \frac{V_i}{V(y)}$$

$$S_T = S_T + \sum_{i \neq j} S_{ij} \tag{12}$$

Fig. 9 shows the variance-based sensitivity for the best SVR model (Table 2) to predict total loss. A Sobol value above 0.05 is generally considered to indicate influential parameters. All parameters have total Sobol indices greater than 0.05, while, except for floor area, their first order Sobol index is below 0.05. This indicates that the parameters' higher-order interaction governs response prediction variance. The variability in floor area is the most influential parameter on total loss variance, as it has the highest first-order (0.24) and total order Sobol (0.81) indices. This influence occurs because both topology and estimated cost are directly related to the floor area. Height is the second most influential parameter, which is consistent with previous research

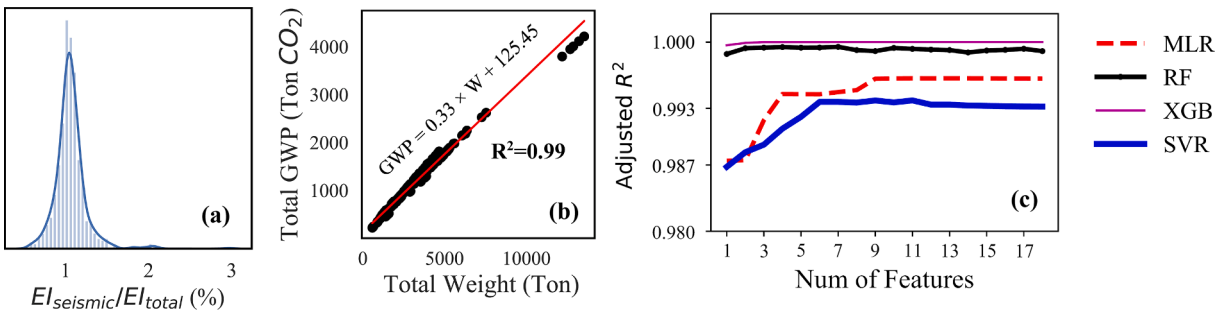

Fig. 8. (a) Histogram of seismic-induced environmental impacts to total environmental impacts, (b) Regression models performance on test set for GWP, and (c) Adjusted R^2 for different number of features in developed surrogate to predict GWP,

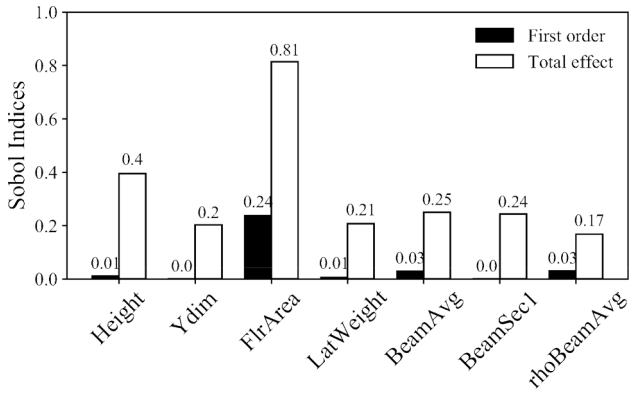

Fig. 9. Variance-based sensitivity analysis of the SVR model predicting total loss.

suggesting height notably impacts concrete frames economic loss [66]. The variance of SVR prediction is also impacted by beams' sizes. This observation matches intuition as the seismic response of special moment frames is governed by yielding in beams, which is related to section dimensions.

6.2. Interpreting SVR

A drawback of using surrogate models such as SVR is the inability to directly interpret results based on model parameters. To overcome this issue, accumulated local effect (ALE) plots were used to demonstrate the influence of features on ML algorithm prediction [82]. ALE divides the feature into intervals and calculates the average in prediction differences as follows [83]:

$$\widehat{f}_{j,ALE}(x) = \sum_{k=1}^{k_j(x)} \frac{1}{n_j(k)} \sum_{i:x_j^{(i)} \in N_j(k)} \left[f\left(z_{k,j}, x_j^{(i)}\right) - f\left(z_{k-1,j}, x_j^{(i)}\right) \right] \tag{13}$$

where N_j is the fine partition of sample range into K intervals. $z_{k,j}$ is the k/K quantile of the empirical distribution of $\{x_{i,j}, i = 1,..n\}$, $n_j(k)$ is the number of training observations in the kth interval $N_j(k)$, x is a particular value of x_j predictor, and j_k is the index of interval where x falls into. The effect is typically centered to have mean effect zero as follows:

$$\widehat{f}_{j,ALE}(x) = \widehat{f}_{j,ALE}(x) - \frac{1}{n}\widehat{f}_{j,ALE}\left(x_j^{(i)}\right) \tag{14}$$

As shown in the ALE plots of Fig. 10, as height and floor area increase, SVR predicts higher total loss, whereas when lateral weight increases, SVR predicts smaller total loss. For other features, the isolated impacts are not substantial, although Fig. 10 suggests that while mid-rise concrete buildings with higher average beam sections have a smaller total loss, larger beam sections on the first floor results in slightly increases total seismic loss. Since beams section are related to yielding mechanism in the frame, this observation implies that using larger beams along the building height leads to a more uniform yielding, which subsequently incurs lower total loss.

Considering the early design of mid-rise concrete frames, the ALE plots suggest that floor area and lateral frames' weight are competing factors to determine the building's total loss. Therefore, a plausible early design scenario is to find the optimum loss value (i.e. local minima) based on floor area and lateral weight. Since lateral weight directly impacts GWP, additional constraints (in terms of an allowable emission level or carbon tax) could be imposed to determine the range of lateral-frame weight that balances the seismic and environmental performance for a given floor area.

6.3. The impact of the initial cost

The total loss values were estimated by assuming a linear cost function (i.e. gross area multiplied by a fixed price per square foot), which implicitly disregards the difference in pricing of different member sizes for the same topology. While such approximation was deemed appropriate [84,85] for the scope of this study, additional sensitivity assessment is warranted to determine its impact on the generalizability of results. Therefore, the SVR surrogate model is trained to predict the total loss for five different building replacement cost of: unity (i.e. imposing no cost estimate, total loss represented as a percentage), linear (i.e. multiplying fixed base price by gross area) weight-adjusted linear: linear cost adjusted by the ratio of total weight per square foot to the average total weight per square foot for the whole inventory to account for member sizing costs, natural logarithm of building gross area multiplied by the base unit price per square foot (i.e. nonlinear relationship of cost and area), square root of building gross area multiplied by the base unit price (an additional nonlinear function to compare with

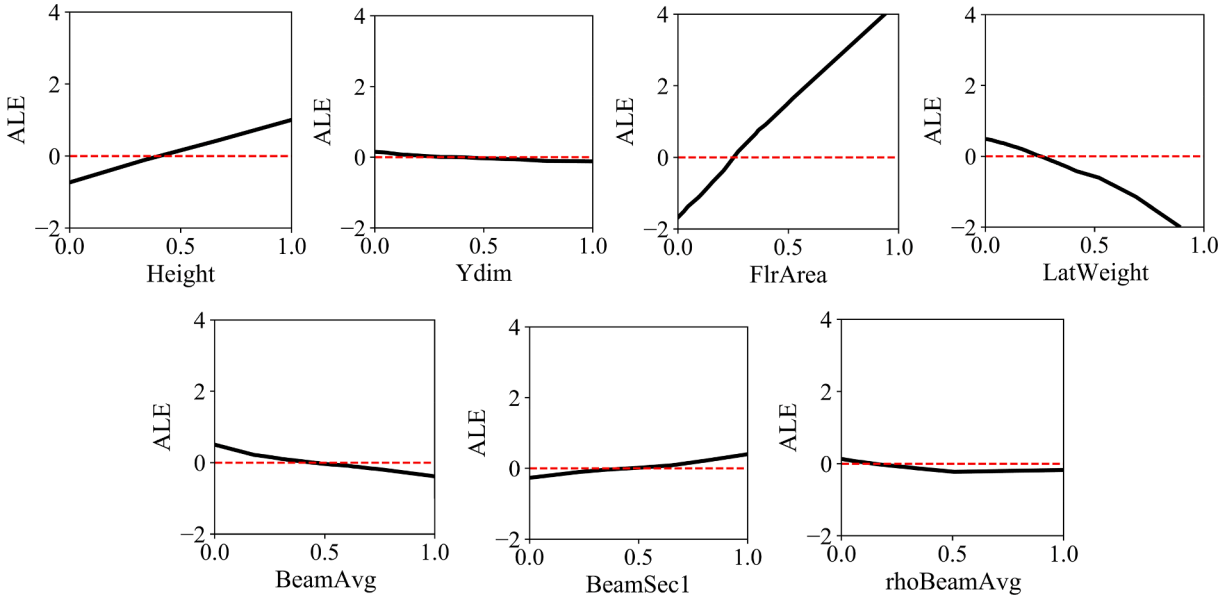

Fig. 10. Accumulated local effect plots for SVR prediction of total loss (feature values are normalized by their range).

logarithmic function).

Fig. 11.a-e and Fig. 11.f compare the impact of different replacement cost estimations on the SVR's performance on the test set and the 10-fold cross-validated adjusted R^2, respectively. The replacement cost significantly impacts SVRs performance, where unity and linear cost functions lead to the worst and best performance with an adjusted R^2 of 0.23 (Fig. 11.a) and 0.94 (Fig. 11.b), respectively. The reasonable accuracy of surrogate models is not limited to assuming a linear cost function, and a nonlinear cost function can generate similar results. Comparing two nonlinear cost functions (i.e. natural logarithmic and square root) shows that for nonlinear cost functions, the SVR model is sensitive to the selected function. Lastly, for the scenario where the fixed price is adjusted based on the amount of used material (i.e. adjusted linear cost function), a reasonable prediction accuracy with an average adjusted R^2 of 0.91 with a standard deviation of 0.07 is observed (Fig. 11.c). This observation suggests that neglecting the impact of frame sizing on cost estimation might be an appropriate assumption, particularly when cost data for different configurations is not easily accessible/ available. Nevertheless, In practice, the final replacement cost will most likely be similar to the cost function 5 (a base price adjusted for larger/smaller sections), and hence, it can be expected that using surrogate models deliver useful results with more refined cost estimates.

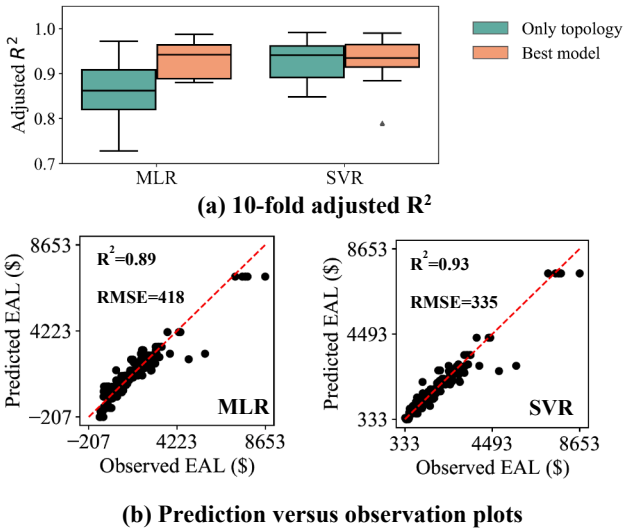

Fig. 12. Comparison of using only topological features and best features for MLR and SVR (a) 10-fold adjusted R2 results for total loss (b) structural and collapse losses results on test set.

6.4. Implication of using only crude topological features

An important question is whether without having any prior information or design experience such as that needed to estimate features like beam average sections, — an engineer could apply surrogate modeling to aid with early design, at the expense of lower accuracy. Therefore, SVR and MLR surrogate models are examined for a feature subsets of only topological features consisting of height, bay length, x-dimension and y-dimension, aspect ratio and floor area. This subset represents the scenario when the structural designer only knows project constraints from AEC discussion and needs to provide some rough estimates for a given structural system. Additionally, MLR and SVR are compared to determine whether for approximate estimates allow a more convenient and interpretable algorithm to replace SVR.

Fig. 12.a compares SVR and MLR performance to predict total loss using 10-fold adjusted R^2. The results indicate that while using topological features results in lower adjusted R^2 in both cases, both models maintained a high adjusted R^2. The SVR model with topological features shows an average adjusted R^2 of 0.92 (0.96 for the best SVR model), whereas MLR shows an average adjusted R^2 of 0.86 (0.92 for the best MLR model). Given that the adjusted R^2 cannot provide a complete picture of surrogate models' predictive abilities, Fig. 12.b compares the predicted loss values to actual values. Compared to the best models results in Table, the RMSE for MLR and SVR are increased by 29% and 18% by excluding design-related features, respectively. An important observation is that at lower loss ranges, in contrast to Fig. 6, MLR now predicts a negative loss value, indicating that MLR model with only topological parameters have high bias and will produce inaccurate results at lower range and underpredict loss at high loss range. Hence, it can be concluded that the advantage of flexible surrogate models are more pronounced for limited information scenarios.

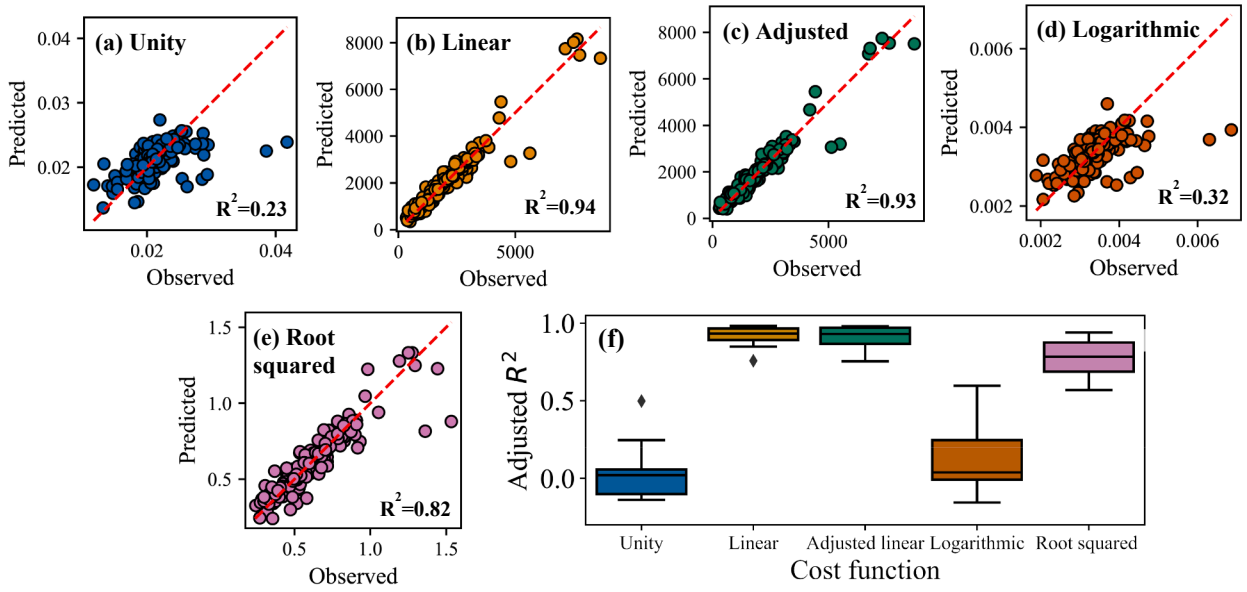

Fig. 11. The impact of (a) unity (b) linear (c) adjusted linear (d) logarithmic (e) root squared cost functions on the SVR prediction. (f) the 10-fold adjusted R2 results for different replacement cost functions.

7. Conclusion

7.1. Summary

This paper investigates the feasibility of implementing data-driven surrogate models to relate crude topological and design parameters to endpoint seismic and environmental measures for a class of buildings in a fixed location. A framework was proposed to develop a multi-dimensional performance inventory by performing seismic vulnerability and life cycle assessments on numerical models of 720 mid-rise concrete office buildings in Charleston, South Carolina. Subsequently, this inventory was used to select and train five surrogate models including multiple linear regression (MLR), random forest (RF), extreme gradient boosting (XGB), support vector machine (SVR), and k-nearest neighbors (KNN). Sensitivity assessments were performed to evaluate most important parameters and study assumptions. The followings summarize the main findings of this study:

- Among different surrogate models, SVR is found to be the best surrogate model to represent the total seismic loss, where the average 10-fold adjusted R^2 for training and testing sets are 0.92 and 0.96, respectively.
- For the considered location, a univariate linear regression on total weight provides an adjusted R^2 of 0.99 and is deemed adequate to represent embodied global warming potential of building inventory.
- Variance-based sensitivity assessment shows that floor area (total Sobol index of 0.81) and building height (total Sobol index of 0.4) are the most influential parameters impacting SVR prediction variability, followed by beam section sizes (total Sobol index of 0.25).
- The influence of early design parameters on SVR prediction is interpreted using accumulated local effects. It was shown that increasing floor area and height resulted in a higher total loss for the mid-rise concrete offices, whereas having larger beam sizes throughout the frame and lateral frames with heavier sections resulted in a lower total loss.
- Using only topological features, SVR surrogate models show reasonable accuracy where the average 10-fold adjusted R^2 was reduced by 1.1%, whereas RMSE was increased by 17.5% for the testing set compared to the best SVR model including design parameters. On the other hand, MLR models with only topological parameters show a 6.8% reduction in adjusted R^2 and a 28.6% increase in RMSE for the testing set. In addition, MLRs exhibit significant bias at low and high losses.
- SVR prediction of total seismic loss is sensitive to the way loss is formulated in terms of building replacement cost, where a linear cost function yields the most accurate model with an average 10-fold adjusted R^2 of 0.91. For unity cost functions, the average 10-fold adjusted R^2 is reduced to only 0.05, indicating that if loss is formulated as percentage, crude topology and design parameters are insufficient for an accurate prediction.

7.2. What is next for structural engineers in the ML-Land?

The results discussed in this paper suggest that it is feasible to build *useful* data-driven models that provide performance data for a given site and class of buildings, even if limited data is available. The word "useful" here is deliberately used in the same context as to how George Box perceived any statistical model; being "*parsimonious*" yet "*illuminating*" [86]. For early design, even with only topologic information, support vector machines explain around 90% of total seismic loss variability for the case study buildings. There are however several important questions to be answered in the future studies. First, performance estimation methods are quite sensitive to hazard characterization [87], structural modeling [68], and even loss calculation methodology [88,89]. It is critical to investigate whether such nuances render surrogate modeling ineffective. For example, if one uses a careful component-based loss method, will the uncertainties in components' fragilities drastically reduce surrogate model accuracy to the extent of not being useful at all? Second, due to the site's seismicity, expected annual loss values were in a quite narrow range, and it poses the question that whether for sites with significantly larger seismicity, such as California, similar conclusions can be made.

Creating surrogate models for a class of buildings does not on its own lead to a performance-based early design: a collaborative plan must be laid out. An avid reader could question how estimating total loss based on floor area and building weight for concrete frames could aid in navigating countless other decisions such as structural and material system choice, envelope selection, etc. The authors believe that developing open performance inventories [25,90] that span different taxonomies, systems and hazards is the key: curated and consistent datasets enable the power of machine learning (ML) as a versatile optimization/prediction tool to a risk-informed design framework that ensures the outcome will meet stakeholders' long-term goals. Without such datasets, surrogate models could not be generalized beyond a single design, or as shown here, a class of buildings. A crowdsourcing culture to share data and models under community-based guidelines will be an important step towards advancing ML-aided design, alongside industry-wide collaboration to integrate practice-based knowledge into ML models through representation of design variability and accurate construction and other required data. Acquiring such holistic datasets will pave the path to explore the generalizability of data-driven surrogate modeling across different building systems and loss methodologies. Developing unified measures to capture properties of building systems (which are similar between different systems), and physics-informed hybrid ML approaches are possible directions to apply data-driven surrogate models in a broader context.

Declaration of Competing Interest

The authors declare that they have no known competing financial interests or personal relationships that could have appeared to influence the work reported in this paper.

Acknowledgement

This research is supported by the U.S. National Science Foundation, Division of Civil, Mechanical, and Material Innovation, through Resilient Sustainable Buildings Award #1455466. Additional support was provided for the first author by the "Disaster Resilience and Risk Management" program at Virginia Tech. The ground motion simulation tools and technical expertise provided by Prof. Martin Chapman are greatly appreciated.

References

[1] Ghobarah A. Performance-based design in earthquake engineering: State of development. Eng Struct 2001. https://doi.org/10.1016/S0141-0296(01)00036-0.
[2] Porter KA. An Overview of PEER's Performance-Based Earthquake Engineering Methodology. 9th Int Conf Appl Stat Probab Civ Eng 2003;273:973–80.
[3] Bertero RD, Bertero VV. Performance-based seismic engineering: The need for a reliable conceptual comprehensive approach. Earthq Eng Struct Dyn 2002;31:627–52. https://doi.org/10.1002/eqe.146.
[4] Günay S, Mosalam KM. PEER performance-based earthquake engineering methodology, revisited. J Earthq Eng 2013. https://doi.org/10.1080/13632469.2013.787377.
[5] Petrini F. Performance-based fire design of complex structures. Int J Lifecycle Perform Eng 2013;1:185. https://doi.org/10.1504/ijlcpe.2013.057562.
[6] Gernay T, Khorasani NE. Recommendations for performance-based fire design of composite steel buildings using computational analysis. J Constr Steel Res 2020. https://doi.org/10.1016/j.jcsr.2019.105906.
[7] Lange D, Devaney S, Usmani A. An application of the PEER performance based earthquake engineering framework to structures in fire. Eng Struct 2014;66:100–15. https://doi.org/10.1016/j.engstruct.2014.01.052.
[8] Alasiri MR, Chicchi R, Varma AH. Post-earthquake fire behavior and performance-based fire design of steel moment frame buildings. J Constr Steel Res 2020;106442.

[9] Memari M, Mahmoud H. Framework for a performance-based analysis of fires following earthquakes. Eng Struct 2018. https://doi.org/10.1016/j.engstruct.2018.05.099.
[10] Attary N, Unnikrishnan VU, van de Lindt JW, Cox DT, Barbosa AR. Performance-Based Tsunami Engineering methodology for risk assessment of structures. Eng Struct 2017. https://doi.org/10.1016/j.engstruct.2017.03.071.
[11] Ciampoli M, Petrini F, Augusti G. Performance-based wind engineering: towards a general procedure. Struct Saf 2011;33:367–78.
[12] Barbato M, Petrini F, Unnikrishnan VU, Ciampoli M. Performance-Based Hurricane Engineering (PBHE) framework. Struct Saf 2013;45:24–35.
[13] Wang Z, Pedroni N, Zentner I, Zio E. Seismic fragility analysis with artificial neural networks: Application to nuclear power plant equipment. Eng Struct 2018;162:213–25.
[14] Seo J, Linzell DG. Horizontally curved steel bridge seismic vulnerability assessment. Eng Struct 2012;34:21–32.
[15] Seo J, Rogers LP. Comparison of curved prestressed concrete bridge population response between area and spine modeling approaches toward efficient seismic vulnerability analysis. Eng Struct 2017;150:176–89.
[16] Chen M, Mangalathu S, Jeon J-S. Bridge fragilities to network fragilities in seismic scenarios: An integrated approach. Eng Struct 2021;237:112212.
[17] Flint MM, Dhulipala SLN, Shahtaheri Y, Tahir H, Ladipo T, Eatherton MR, et al. Developing a Decision Framework for Multi-Hazard Design of Resilient, Sustainable Buildings. 1st Int. Conf. Nat. Hazards Infrastruct. 2016.
[18] Shahtaheri Y, Flint MM, de la Garza JM. Sustainable Infrastructure Multi-Criteria Preference assessment of aLternatives for Early Design. Autom Constr 2018;96:16–28. https://doi.org/10.1016/j.autcon.2018.08.022.
[19] Østergård T, Jensen RL, Maagaard SE. Building simulations supporting decision making in early design - A review. Renew Sustain Energy Rev 2016. https://doi.org/10.1016/j.rser.2016.03.045.
[20] Rezaee R, Brown J, Haymaker J, Augenbroe G. A new approach to performance-based building design exploration using linear inverse modeling. J Build Perform Simul 2019;12:246–71. https://doi.org/10.1080/19401493.2018.1507046.
[21] Ochoa CE, Capeluto IG. Advice tool for early design stages of intelligent facades based on energy and visual comfort approach. Energy Build 2009;41:480–8. https://doi.org/10.1016/j.enbuild.2008.11.015.
[22] O'Reilly GJ, Calvi GM. Conceptual seismic design in performance-based earthquake engineering. Earthq Eng Struct Dyn 2019;48:389–411.
[23] Shahnazaryan D, O'Reilly GJ. Integrating expected loss and collapse risk in performance-based seismic design of structures. Bull Earthq Eng 2021;19:987–1025.
[24] O'Reilly GJ, Calvi GM. Quantifying seismic risk in structures via simplified demand–intensity models. Bull Earthq Eng 2020;18:2003–22.
[25] Zaker Esteghamati M, Lee J, Musetich M, Flint MM. INSSEPT: An open-source relational database of seismic performance estimation to aid with early design of buildings. Earthq Spectra 2020. https://doi.org/10.1177/8755293020919857.
[26] Guan X, Burton H, Shokrabadi M, Yi Z. Seismic Drift Demand Estimation for Steel Moment Frame Buildings: From Mechanics-Based to Data-Driven Models. J Struct Eng 2021;147:4021058.
[27] O'Reilly GJ, Monteiro R, Nafeh AMB, Sullivan TJ, Calvi GM. Displacement-based framework for simplified seismic loss assessment. J Earthq Eng 2020;24:1–22.
[28] Amini A, Abdollahi A, Hariri-Ardebili MA. Lall UCopula-based reliability and sensitivity analysis of aging dams: Adaptive Kriging and polynomial chaos Kriging methods. Appl Soft Comput 2021:107524.
[29] Soraghi A, Huang Q. Probabilistic prediction model for RC bond failure mode. Eng Struct 2021;233:111944.
[30] Momeni H, Basereh S, Okumus P, Ebrahimkhanlou A. Surface crack detection in concrete structures using video processing techniques. Heal. Monit. Struct. Biol. Syst. XV, vol. 11593, International Society for Optics and Photonics; 2021, p. 115932B.
[31] Sepasdar R, Karpatne A, Shakiba M. A data-driven approach to full-field damage and failure pattern prediction in microstructure-dependent composites using deep learning. ArXiv Prepr ArXiv210404485 2021.
[32] Seo J, Park H. Probabilistic seismic restoration cost estimation for transportation infrastructure portfolios with an emphasis on curved steel I-girder bridges. Struct Saf 2017;65:27–34.
[33] Seo J, Dueñas-Osorio L, Craig JI, Goodno BJ. Metamodel-based regional vulnerability estimate of irregular steel moment-frame structures subjected to earthquake events. Eng Struct 2012;45:585–97.
[34] Seo J, Kim YJ, Zandyavari S. Response surface Metamodel-based performance reliability for reinforced concrete beams Strengthened with FRP Sheets. Spec Publ 2015;304:1–20.
[35] Du A, Padgett JE. Investigation of multivariate seismic surrogate demand modeling for multi-response structural systems. Eng Struct 2020. https://doi.org/10.1016/j.engstruct.2020.110210.
[36] Seo J, Linzell DG. Use of response surface metamodels to generate system level fragilities for existing curved steel bridges. Eng Struct 2013. https://doi.org/10.1016/j.engstruct.2013.03.023.
[37] Mangalathu S, Heo G, Jeon JS. Artificial neural network based multi-dimensional fragility development of skewed concrete bridge classes. Eng Struct 2018;162:166–76. https://doi.org/10.1016/j.engstruct.2018.01.053.
[38] Ataei N, Padgett JE. Fragility surrogate models for coastal bridges in hurricane prone zones. Eng Struct 2015;103:203–13. https://doi.org/10.1016/j.engstruct.2015.07.002.
[39] Zhong J, Wan HP, Yuan W, He M, Ren WX. Risk-informed sensitivity analysis and optimization of seismic mitigation strategy using Gaussian process surrogate model. Soil Dyn Earthq Eng 2020. https://doi.org/10.1016/j.soildyn.2020.106284.
[40] Bernier C, Padgett JE. Fragility and risk assessment of aboveground storage tanks subjected to concurrent surge, wave, and wind loads. Reliab Eng Syst Saf 2019. https://doi.org/10.1016/j.ress.2019.106571.
[41] Le V, Caracoglia L. A neural network surrogate model for the performance assessment of a vertical structure subjected to non-stationary, tornadic wind loads. Comput Struct 2020. https://doi.org/10.1016/j.compstruc.2020.106208.
[42] Javidan MM, Kang H, Isobe D, Kim J. Computationally efficient framework for probabilistic collapse analysis of structures under extreme actions. Eng Struct 2018. https://doi.org/10.1016/j.engstruct.2018.06.022.
[43] Fang C, Tang H, Li Y, Zhang J. Stochastic response of a cable-stayed bridge under non-stationary winds and waves using different surrogate models. Ocean Eng 2020. https://doi.org/10.1016/j.oceaneng.2020.106967.
[44] Micheli L, Hong J, Laflamme S, Alipour A. Surrogate models for high performance control systems in wind-excited tall buildings. Appl Soft Comput J 2020. https://doi.org/10.1016/j.asoc.2020.106133.
[45] Li S, Caracoglia L. Surrogate Model Monte Carlo simulation for stochastic flutter analysis of wind turbine blades. J Wind Eng Ind Aerodyn 2019. https://doi.org/10.1016/j.jweia.2019.02.004.
[46] Wilkie D, Galasso C. Gaussian process regression for fatigue reliability analysis of offshore wind turbines. Struct Saf 2021;88:102020.
[47] Zou J, Welch DP, Zsarnoczay A, Taflanidis A, Deierlein GG. Surrogate Modeling for the Seismic Response Estimation of Residential Wood Frame Structures. Proc. 17th World Conf. Earthq. Eng. Japan 2020.
[48] Hwang SH, Mangalathu S, Shin J, Jeon JS. Machine learning-based approaches for seismic demand and collapse of ductile reinforced concrete building frames. J Build Eng 2020. https://doi.org/10.1016/j.jobe.2020.101905.
[49] Mitropoulou CC, Papadrakakis M. Developing fragility curves based on neural network IDA predictions. Eng Struct 2011. https://doi.org/10.1016/j.engstruct.2011.07.005.
[50] Gidaris I, Taflanidis AA, Mavroeidis GP. Kriging metamodeling in seismic risk assessment based on stochastic ground motion models. Earthq Eng Struct Dyn 2015. https://doi.org/10.1002/eqe.2586.
[51] Möller O, Foschi RO, Rubinstein M, Quiroz L. Seismic structural reliability using different nonlinear dynamic response surface approximations. Struct Saf 2009. https://doi.org/10.1016/j.strusafe.2008.12.001.
[52] Gentile R, Galasso C. Gaussian process regression for seismic fragility assessment of building portfolios. Struct Saf 2020;87:101980.
[53] Micheli L, Alipour A, Laflamme S. Multiple-Surrogate Models for Probabilistic Performance Assessment of Wind-Excited Tall Buildings under Uncertainties. ASCE-ASME J Risk Uncertain Eng Syst Part A Civ Eng 2020. https://doi.org/10.1061/ajrua6.0001091.
[54] Moehle JP, Hooper JD, Lubke CD. Seismic Design of Reinforced Concrete Special Moment Frames: A Guide for Practicing Engineers. NEHRP Seism Des Tech Br No 1 (NIST GCR 8-917-1) 2008.
[55] Guan X, Burton H, Sabol T. Python-based computational platform to automate seismic design, nonlinear structural model construction and analysis of steel moment resisting frames. Eng Struct 2020. https://doi.org/10.1016/j.engstruct.2020.111199.
[56] Liel AB, Haselton CB, Deierlein GG. Seismic Collapse Safety of Reinforced Concrete Buildings. II: Comparative Assessment of Nonductile and Ductile Moment Frames. J Struct Eng 2011;137:492–502. https://doi.org/10.1061/(ASCE)ST.1943-541X.0000275.
[57] American Society of Civil Engineers. Minimum design loads for buildings and other structures, ASCE standard, ASCE Stand 2010:608. doi: 10.1061/9780784412916.
[58] ACI Committee 318. Building Code Requirements for Structural Concrete (ACI 318-08). vol. 2007. 2008. doi: 10.1016/0262-5075(85)90032-6.
[59] McKenna F. OpenSees: A framework for earthquake engineering simulation. Comput Sci Eng 2011. https://doi.org/10.1109/MCSE.2011.66.
[60] Haselton CB, Liel AB, Lange ST. Beam-Column Element Model Calibrated for Predicting Flexural Response Leading to Global Collapse of RC Frame Buildings. Peer 2007;2008:03.
[61] Zaker Esteghamati M, Banazadeh M, Huang Q. The effect of design drift limit on the seismic performance of RC dual high-rise buildings. Struct Des Tall Spec Build 2018:e1464.. https://doi.org/10.1002/tal.1464.
[62] Zaker Esteghamati M, Bahrampouri M, Rodriguez-Marek A. The impact of hazard-consistent ground motion scenarios selection on structural seismic risk estimation. Geotech Eng Extrem Events 2021.
[63] ASCE, SEI. Commentary for Chapters 11-22 (Seismic) ASCE 7 - 10. Minim. Des. Loads Build. Other Struct, 2013, p. 608. doi: 10.1061/9780784412916.
[64] FEMA. Hazus-MH 2.1 Earthquake Model Technical Manual 2011:1–718.
[65] Zaker Esteghamati M, Farzampour A. Probabilistic seismic performance and loss evaluation of a multi-story steel building equipped with butterfly-shaped fuses. J Constr Steel Res 2020;172:106187. https://doi.org/10.1016/j.jcsr.2020.106187.
[66] Ramirez CM, Liel AB, Mitrani-Reiser J, Haselton CB, Spear AD, Steiner J, et al. Expected earthquake damage and repair costs in reinforced concrete frame buildings. Earthq Eng Struct Dyn 2012. https://doi.org/10.1002/eqe.2216.
[67] Baker JW. Efficient analytical fragility function fitting using dynamic structural analysis. Earthq Spectra 2015. https://doi.org/10.1193/021113EQS025M.
[68] Gokkaya BU, Baker JW, Deierlein GG. Quantifying the impacts of modeling uncertainties on the seismic drift demands and collapse risk of buildings with implications on seismic design checks. Earthq. Eng. Struct. Dyn. 2016. https://doi.org/10.1002/eqe.2740.
[69] RSMeans. RSMeans Data Online Core: Building Construction Costs. n.d. https://www.rsmeans.com/products/online/core.aspx (accessed June 3, 2021).

[70] Gagnon R, Gosselin L, Armand Decker S. Performance of a sequential versus holistic building design approach using multi-objective optimization. J Build Eng 2019. https://doi.org/10.1016/j.jobe.2019.100883.
[71] Shahtaheri Y, Flint MM, de la Garza JM. A multi-objective reliability-based decision support system for incorporating decision maker utilities in the design of infrastructure. Adv Eng Informatics 2019;42:100939. https://doi.org/10.1016/j.aei.2019.100939.
[72] Institute AS. Athena Impact Estimator for Buildings V 4.5 Users Manual, Software and Database Overview. 2013.
[73] (ATC) ATC. Development of next generation performance-based seismic design procedures for new and existing buildings 2009.
[74] Junnila S, Horvath A, Guggemos AA. Life-Cycle Assessment of Office Buildings in Europe and the United States. J Infrastruct Syst 2006. https://doi.org/10.1061/(asce)1076-0342(2006)12:1(10).
[75] Chau CK, Leung TM, Ng WY. A review on life cycle assessment, life cycle energy assessment and life cycle carbon emissions assessment on buildings. Appl Energy 2015. https://doi.org/10.1016/j.apenergy.2015.01.023.
[76] Hasik V, Chhabra JPS, Warn GP, Bilec MM. Review of approaches for integrating loss estimation and life cycle assessment to assess impacts of seismic building damage and repair. Eng Struct 2018;175:123–37. https://doi.org/10.1016/j.engstruct.2018.08.011.
[77] Moustapha M, Bourinet J-M, Guillaume B, Sudret B. Comparative Study of Kriging and Support Vector Regression for Structural Engineering Applications. ASCE-ASME J Risk Uncertain Eng Syst Part A Civ Eng 2018. https://doi.org/10.1061/ajrua6.0000950.
[78] Hastie T, Tibshirani R, Friedman J. Elements of Statistical Learning. 2nd ed. 2009.
[79] Chen T, Guestrin C. XGBoost: A scalable tree boosting system. Proc. ACM SIGKDD Int Conf. Knowl. Discov. Data Min. 2016. https://doi.org/10.1145/2939672.2939785.
[80] Fan GF, Guo YH, Zheng JM, Hong WC. Application of the weighted k-nearest neighbor algorithm for short-term load forecasting. Energies 2019. https://doi.org/10.3390/en12050916.
[81] Oakley JE, O'Hagan A. Probabilistic sensitivity analysis of complex models: A Bayesian approach. J R Stat Soc Ser B Stat Methodol 2004. https://doi.org/10.1111/j.1467-9868.2004.05304.x.
[82] Apley DW, Zhu J. Visualizing the effects of predictor variables in black box supervised learning models. J R Stat Soc Ser B Stat Methodol 2020. https://doi.org/10.1111/rssb.12377.
[83] Molnar C. Interpretable Machine Learning. A Guide for Making Black Box Models Explainable. Book 2019.
[84] Welsh-Huggins S, Liel AB. Is a stronger building also greener? influence of seismic design decisions on building life-cycle economic and environmental impacts. In: Proc. 6th Int. Symp. Life-Cycle Civ. Eng. Delft, Netherlands; 2016.
[85] Nikellis A, Sett K, Whittaker AS. Multihazard Design and Cost-Benefit Analysis of Buildings with Special Moment-Resisting Steel Frames. J Struct Eng 2019;145:4019031.
[86] Box GEP. Robustness in the strategy of scientific model building. Robustness Stat.: Elsevier; 1979. p. 201–36.
[87] Kwon OS, Elnashai A. The effect of material and ground motion uncertainty on the seismic vulnerability curves of RC structure. Eng Struct 2006;28:289–303. https://doi.org/10.1016/j.engstruct.2005.07.010.
[88] Baker JW, Cornell CA. Uncertainty propagation in probabilistic seismic loss estimation. Struct Saf 2008. https://doi.org/10.1016/j.strusafe.2006.11.003.
[89] Bazzurro P, Luco N. Effects of different sources of uncertainty and correlation on earthquake-generated losses. Aust J Civ Eng 2007. https://doi.org/10.1080/14488353.2007.11463924.
[90] Guan M, EERI X, Burton M, EERI H, Shokrabadi M. A database of seismic designs, nonlinear models, and seismic responses for steel moment-resisting frame buildings. Earthq Spectra 2020. https://doi.org/10.1177/8755293020971209.